Dye-Sensitized Ternary Copper Chalcogenide Nanocrystals: Optoelectronic Properties, Air Stability, and Photosensitivity

Sonam Maiti,[†,‡] Santanu Maiti,[‡] Ali Hossain Khan,[§,∥] Andreas Wolf,[⊥] Dirk Dorfs,[⊥]
Iwan Moreels,[§,∥] Frank Schreiber,[‡,#] and Marcus Scheele[*,†,#]

[†]Institute of Physical and Theoretical Chemistry, University of Tübingen, Auf der Morgenstelle 18, 72076 Tübingen, Germany
[‡]Institute of Applied Physics, University of Tübingen, Auf der Morgenstelle 10, 72076 Tübingen, Germany
[§]Istituto Italiano di Tecnologia, Via Morego 30, 16163 Genova, Italy
[∥]Department of Chemistry, Ghent University, Krijgslaan 281-S3, 9000 Gent, Belgium
[⊥]Institute of Physical Chemistry and Electrochemistry, Leibniz Universität Hannover, Callinstr. 3A, 30167 Hannover, Germany
[#]Center for Light-Matter Interaction, Sensors & Analytics LISA+, University of Tübingen, Auf der Morgenstelle 15, 72076 Tübingen, Germany

S Supporting Information

ABSTRACT: We report on the effect of ligand exchange of $Cu_2Se_yS_{1−y}$ and Cu_2Se nanocrystals (NCs) with the organic π-system cobalt β-tetraaminophthalocyanine (CoTAPc) and analyze the changes in the structural, optical, and electric properties of thin films of these hybrid materials. A strong ligand interaction with the surface of the NCs is revealed by UV/vis absorption and Raman spectroscopy. Grazing-incidence small-angle X-ray scattering studies show a significant contraction in the interparticle distance upon ligand exchange. For copper-deficient $Cu_{2−x}Se$, this contraction has a negligible effect on electric transport, whereas for copper-deficient $Cu_{2−x}Se_yS_{1−y}$, the conductivity increases by 8 orders of magnitude and results in metal-like temperature-dependent transport. We discuss these differences in the light of varying contributions of electronic vs ionic transport in the two materials and highlight their effect on the stability of the transport properties under ambient conditions. With photocurrent measurements, we demonstrate high optical responsivities of 200−400 A W$^{−1}$ for CoTAPc-capped $Cu_2Se_yS_{1−y}$ and emphasize the beneficial role of the organic π-system in this respect, which acts as an electronic linker and an optical sensitizer at the same time.
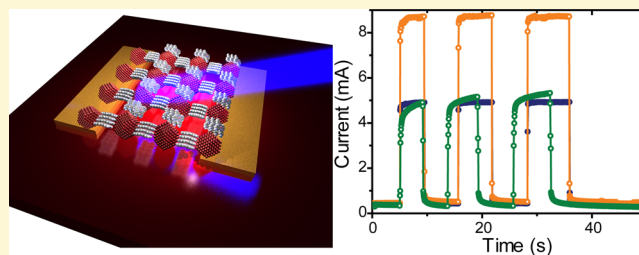
1. INTRODUCTION

Copper chalcogenide nanocrystals (NCs) have become a subject of intense research as possible alternatives to the more toxic Cd or Pb-based counterparts for optoelectronic applications such as solar cells or photocatalysts but also as thermoelectric converters, gas sensors, optical filters, superionic conductors, and electro-optical devices.[1−13] A majority of these investigations focused on the binary compounds copper selenide (Cu_2Se) and copper sulfide (Cu_2S) with variable Cu(I) deficiency (e.g., $Cu_{2−x}Se$, $0.00 \leq x \leq 0.6$) and tailored charge carrier concentration as well as charge carrier concentration-dependent localized plasmon resonance frequency (LSPR).[11,14−23] Introducing Cu(I) vacancies is readily afforded by oxidizing parts of the chalcogenide sublattice into the (−I)-state, which leads to loss of Cu(I)-ions and release of free holes in the NC core.[24] More recently, the ternary alloy, $Cu_2Se_yS_{1−y}$, has been studied to some extent, for instance as a precursor in the synthesis of $Cu_2ZnSn(Se_yS_{1−y})_4$ NCs with relevance for photovoltaic applications.[7,8,25−30] In particular, with respect to the oxidation-sensitive Cu_2Se system, it has been argued that $Cu_2Se_yS_{1−y}$ may have similar optoelectronic

properties, however, with improved stability in air.[31,32] For binary, copper-deficient copper chalcogenide NCs, $Cu_{2−x}Se$ and $Cu_{2−x}S$, several studies have been conducted to increase the electronic coupling in thin films of these materials, for instance by removing the native ligand with smaller molecules or anions, by thermal decomposition of the insulating ligand sphere, or by thermal doping.[3,5,19,20,33−40] Specifically for $Cu_{2−x}Se$ NCs, several groups have reported that high electric conductivities (up to 25 S cm$^{−1}$) may also be obtained without such postsynthetic ligand exchange, indicating that charge carrier transport in these NCs potentially follows a different mechanism than that in copper sulfide, where ligand exchange is usually necessary.[41−44] From the perspective of tailoring the optoelectronic properties of copper chalcogenide NCs by their surface chemistry, such ligand-independent transport characteristics are undesirable. However, the electric conductivities in
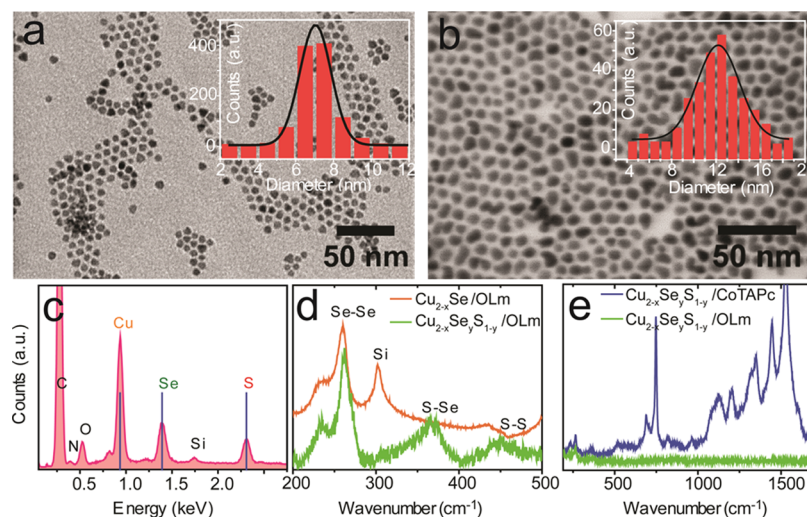
Figure 1. TEM images of (a) 7.0 ± 0.8 nm $Cu_2S_ySe_{1-y}$ NCs and (b) 12.2 ± 1.9 nm Cu_2Se NCs. (c) EDX spectrum of the $Cu_2S_ySe_{1-y}$ NCs. (d) Raman spectra of as-prepared Cu_2Se and $Cu_2Se_yS_{1-y}$ nanocrystal thin films (orange curve and green curve, respectively). (e) Raman spectra of CuSeS nanocrystal thin films before and after ligand exchange (green curve and blue curve, respectively).

Cu_2Se NCs are often found to be larger than in comparable Cu_2S NCs.[37,45]

The present study is motivated by the hypothesis that alloying Cu_2S into Cu_2Se may combine the ligand-tunable optoelectronic of pure Cu_2S with the high electric conductivity of pure Cu_2Se. To this end, we compare the optical and electrical properties of Cu_2Se and $Cu_{2-x}Se$ with $Cu_2Se_yS_{1-y}$ and $Cu_{2-x}Se_yS_{1-y}$, assess the different sensitivity to oxidation in air, and the effect of ligand exchange with the organic π-system cobalt β-tetraaminophthalocyanine (CoTAPc). We show that only the ternary alloy exhibits stable electric transport properties in air. Electrical conductivities >1 S cm^{-1} and an increasing resistivity with increasing temperature indicate highly efficient charge carrier transport in CoTAPc-functionalized $Cu_{2-x}Se_yS_{1-y}$ NC thin films. We demonstrate an optical responsivity of 400 A W^{-1} under 637 nm photoexcitation, which is an exceptionally large photosensitivity for this material. We argue that this is enabled by the hybrid nature of the presented material, in which the organic π-system acts as the photosensitizer and the network of NCs provides the channel for fast transport of the photoexcited charges.

2. METHODS

2.1. Synthesis of Cu_2Se Nanocrystals. A synthesis method adapted from Deka et al. has been used to produce quasispherical Cu_2Se NCs.[43] Standard Schlenk line techniques were applied for synthesis and purification. A mixture of 15 mL of 1-octadecene (ODE) and 15 mL of oleylamine (OLm) is degassed under vacuum at 115 °C for 3 h. The mixture is cooled to room temperature, and under argon flow, 297 mg of copper(I) chloride (CuCl, 3 mmol) is added. For an additional 15 min, the mixture is heated to reflux under vacuum. Subsequently, the flask is filled with argon and the temperature is raised to 300 °C in 5−6 min. The selenium (Se) precursor solution is prepared by dissolving Se (117 mg, 1.5 mmol) in degassed OLm (9 mL) and refluxing under vacuum for 30 min (115 °C). The flask is again filled with argon and the mixture is left stirring at 190−200 °C until all Se is dissolved. Upon dissolution, the temperature is raised to 230 °C for 20 min. To transfer the precursor solution with a glass syringe, the solution is cooled to 150 °C. The Se solution is rapidly injected into the copper precursor solution. The temperature of the reaction mixture is allowed to recover to 290 °C within approximately 2−3 min. The reaction is quenched 15 min after the injection. At 150 °C, toluene (20 mL) is injected to prevent

agglomeration. The particles are precipitated from the growth solution with ethanol (20 mL) and methanol (10 mL) and centrifuged (3700g, 20 min). The precipitate is resuspended in toluene (20 mL) by ultrasonication (5 min). After 12 h, the solution is centrifuged again (3700g, 20 min) to remove aggregates. The supernatant is collected and used for all further experiments.

2.2. Synthesis of $Cu_2Se_yS_{1-y}$ Nanocrystals. The Se-precursor solution is prepared according to the method reported by Lesnyak et al.[2] 158 mg of Se powder (2 mmol) is mixed with 1 mL of 1-dodecanethiol (DDT) and 1 mL of OLm and is heated for 1 h at 100 °C under a nitrogen atmosphere. The resultant, brown alkyl ammonium selenide solution is cooled to room temperature and stored in a nitrogen-filled glass vial.

In a three-necked round-bottom flask, 262 mg of copper(II) acetylacetonate $[Cu(acac)_2]$ (1 mmol) is mixed with 3.5 mL of DDT and 10 mL of OLm, and the mixture is degassed under vacuum with vigorous stirring at 70 °C for 1 h. Then, the flask is filled with nitrogen and quickly heated to 220 °C. After complete dissolution, $Cu(acac)_2$ forms a clear yellow solution. At this temperature, a mixture of 0.5 mL of the Se-precursor with 1.5 mL of DDT is swiftly injected into the flask leading to immediate color change from yellow to brown. The reaction mixture is kept at 220 °C for 30 min. The nanocrystals are precipitated under an inert gas atmosphere by centrifugation of the crude reaction mixture with subsequent dissolution of the precipitate in chloroform.

2.3. Thin-Film Preparation and Ligand Exchange. NC thin films were prepared by assembly at the dimethylsulfoxide/N_2 interface under inert conditions in a glovebox. The fabrication process and ligand exchange were carried out in a home-built Teflon chamber according to our previously reported method.[5]

2.4. Instrumentation. Scanning transmission electron microscopy (STEM, Hitachi SU 8030 microscope operating at 30 kV) is employed to determine the particle size and shape. Optical measurements are performed on solid-state films on glass substrates using a UV−vis−NIR spectrometer (Agilent Technologies, Cary 5000). Grazing-incidence small-angle X-ray scattering (GISAXS)[6,46−49] is carried out with a laboratory instrument (Xeuss 2.0, Xenocs, France) using Cu Kα radiation (λ = 1.5418 Å). The samples are probed with a focused X-ray beam of size 0.5 × 0.5 mm^2 at an incidence angle of 0.22°. The GISAXS images are collected with a 2D Pilatus 300 K, having 487 × 619 pixels. The detector is placed at a distance of 2496 mm, determined using Ag-behenate as the reference sample. X-ray diffraction (XRD) data from the sample is collected in a laboratory source (Cu Kα; GE Inspection Technologies, Germany). Raman spectra are acquired using a Horiba Jobin Yvon Labram HR
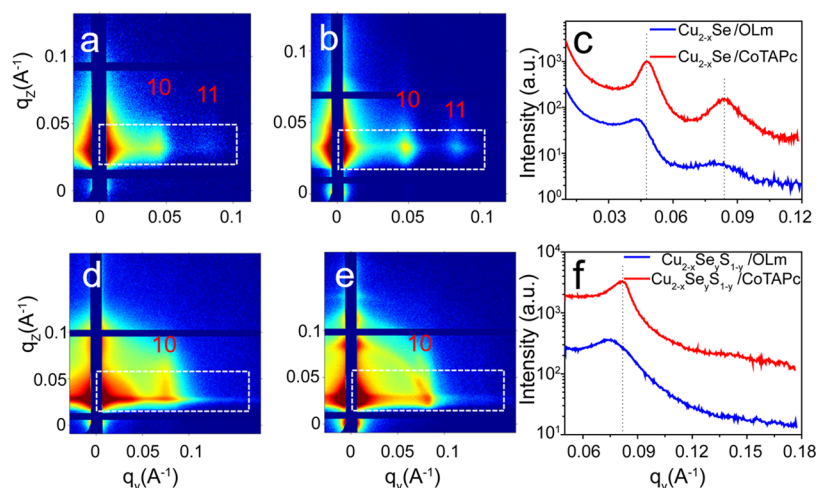
Figure 2. GISAXS patterns of self-assembled (a) Cu_2Se/OLm, (b) $Cu_2Se/CoTAPc$, (d) $Cu_2Se_yS_{1-y}/OLm$, and (e) $Cu_2Se_yS_{1-y}/CoTAPc$ films (c) and (f) extracted line profiles from the corresponding GISAXS images on the left in (a)/(b) and (d)/(e), respectively, as a function of the in-plane scattering vector q_y. To improve the statistics of the line profiles, the region of interest (white dotted box) was integrated along the q_z direction.

800 spectrometer with a CCD-1024 × 256-OPEN-3S9 detector. Excitation for Raman is performed using a He/Ne laser (wavelength 633 nm). Electrical measurements are performed in a glovebox at room temperature with a homemade probe station using a Keithley 2634B dual source-meter unit, controlled by the included test script builder program. The NC films after ligand exchange are deposited on commercially available bottom-gate, bottom-contact transistor substrates (Fraunhofer Institute for Photonic Microsystems, Dresden, Germany) with interdigitated Au electrodes of 10 mm width and 2.5 μm channel length followed by annealing at 250 °C for 2 h under a nitrogen atmosphere. The temperature-dependent charge transport properties and the photoresponse of the NC thin films are measured in a Lake-Shore CRX-6.5K probe station at a pressure of 5×10^{-6} mbar, equipped with a Keithley 2636B dual source-meter unit and a Lake-Shore temperature controller (model 336). As an excitation source, single-mode fiber-pigtailed laser diodes operated by a compact laser diode controller CLD1010 by Thorlabs were used: A 638 nm laser diode with a maximal output power of 70 mW and a 408 nm diode with a maximal output power of 30 mW. Losses to this theoretical optical power output due to scattering, inefficient coupling into the optical fiber, decollimation of the beam, etc. were determined by a calibration sample and an optical power meter to obtain the total absorbed optical power at the sample surface.

3. RESULTS AND DISCUSSION

The TEM images in Figure 1a,b depict the morphologies of the as-synthesized alloyed $Cu_2Se_yS_{1-y}$ and $Cu_{2-x}Se$ NCs with relatively uniform sizes of 7.0 ± 0.8 and 12.2 ± 1.9 nm, respectively. All NCs appear well separated by the native OLm capping ligand. Powder X-ray diffraction reveals that the $Cu_2Se_yS_{1-y}$ NCs are in the hexagonal phase (Figure S1).[8] We determine the composition of the alloyed NCs by energy-dispersive X-ray (EDX) spectroscopy as $Cu_{2.2}Se_{0.68}S_{0.32}$ (Figure 1c). We note that colloidal NCs often exhibit an excess of cations on the surface, such that the actual stoichiometry of the inner core may contain less copper than that suggested by our EDX result. Figure 1d shows the Raman spectra for solid-state films of both NC materials coated with the native OLm ligand. In good agreement with previous reports, the most intense resonance peak is observed at around 260 cm^{-1} for both samples, corresponding to the Se−Se stretching vibration.[21,50] For the films composed of the ternary $Cu_2Se_yS_{1-y}$ NCs, two additional peaks are observed, one at 450 cm^{-1} corresponding to the S−S stretching mode and another peak at 368 cm^{-1} due

to the S−Se stretching mode.[51] Consistent with the EDX data, the intensity of the Se−Se band is much stronger than that of the S−S and S−Se stretching vibrations, suggesting that the alloy is rich in selenium.

To enhance the chemical and electronic coupling in solid-state films of both NC materials, we exchange the native OLm ligand with the multidendate cross-linker CoTAPc. We choose this linker because earlier reports have shown that tetraaminophthalocyanines are suitable for replacing oleyl-amine from the surface of $Cu_{1.1}S$ NCs and drastically improve the charge carrier transport.[5] The ligand-exchanged NC films exhibit a smooth surface with an average height difference of 3−4 NCs and 1 NC monolayer for $Cu_2Se_yS_{1-y}$ and Cu_2Se, respectively (Figure S2). We monitor the effect of this ligand exchange by Raman spectroscopy in Figure 1e. (This figure exemplifies the exchange for $Cu_2Se_yS_{1-y}$ NCs, but the same spectral features between 700 and 1700 cm^{-1} are also obtained with Cu_2Se after ligand exchange.) In accordance with previous studies, we interpret the strong bands appearing at 747, 1124, 1202, 1337, 1447, 1530, and 1605 cm^{-1} with vibrational modes of CoTAPc, which is a supporting piece of evidence for the presence of a new linker in the NC film.[52] The peaks at 300 and 513 cm^{-1} belong to the Si substrate. Fourier-transform infrared spectroscopy furthermore reveals significant changes after exposure to CoTAPc, most notably the disappearance of characteristic OLm vibrations at 1660 and 3350 cm^{-1}. (For details, see Figure S3 in the Supporting Information.)

We determine the structural details of the ensemble of the two NC samples as well as the effect of ligand exchange with CoTAPc by GISAXS in Figure 2. The intense in-plane scattering truncation rods extended along the q_z-direction indicate the formation of superlattices with long-range in-plane order. For OLm-capped $Cu_{2-x}Se$ NCs (Figure 2a+c), we find the first-order in-plane correlation peak at $q_y = 0.043$ Å^{-1}, a second order peak at $q_y = 0.078$ Å^{-1}, and a barely visible third signal at $q_y \approx 0.9$ Å^{-1}. These relative positions in q_y can be interpreted as the formation of a hexagonal lattice (e.g., $q_1/q_2/q_3 = 1:\sqrt{3}:2$) with in-plane lattice constant $a = 16.8 \pm 0.1$ nm. After ligand exchange with CoTAPc (Figure 2b+c), the in-plane correlation peaks shift to higher values, that is, smaller lattice constants, and we find $q_y = 0.048, 0.084$ Å^{-1}, and a shoulder at 0.096 Å^{-1}. These values are again in agreement

with a hexagonal lattice, but with a contracted in-plane lattice constant $a = 15.1 \pm 0.1$ nm. We attribute the contraction of 1.7 nm to the replacement of OLm by the smaller CoTAPc ligand. The improved signal-to-background ratio after ligand exchange indicates a higher degree of long-range order as a result of cross-linking with the rigid organic π-system. With respect to the average particle diameter of 12.2 ± 1.9 nm (Figure 1b), the interparticle spacing before ligand exchange is 4.6 ± 1.9 nm, which can be interpreted with two adjacent, nonintercalated ligand spheres of OLm. After cross-linking with CoTAPc, the interparticle spacing is reduced to 2.9 ± 1.9 nm, which is equivalent to 1−2 times the molecular length of CoTAPc. Since the exact binding mode of CoTAPc to the surface of the NCs is not known, the latter finding could either be explained with a side-on binding of stacks of CoTAPc or with head-to-tail cross-linking of a CoTAPc monolayer.

Similar GISAXS patterns are also obtained for $Cu_{2-x}Se_yS_{1-y}$ before and after ligand exchange with CoTAPc (Figure 2d+e). The first-order correlation peak shifts from 0.074 $Å^{-1}$ with OLm functionalization to 0.082 $Å^{-1}$ after ligand exchange (Figure 2f). Under the assumption of a hexagonal lattice, this corresponds to a center-to-center distance between the NCs of 9.8 ± 0.1 nm for OLm functionalization and 8.8 ± 0.1 nm for CoTAPc as the ligand. With a particle diameter of 7.0 ± 0.8 nm, the interparticle distances are 2.8 ± 0.8 nm for OLm and 1.8 ± 0.8 nm for CoTAPc. The latter result may be viewed as indirect supporting evidence that CoTAPc binds preferentially in a head-to-tail cross-linking manner between the surfaces of two adjacent NCs as the width of the ligand sphere is precisely 1 molecular length of CoTAPc.

For charge transport studies, we deposit both copper chalcogenide NC films on silicon oxide substrates with prepatterned Au contacts and record the two-point probe current−voltage (I−V) characteristics at room temperature. In Figure 3a+b, we focus on a comparison of the I/V characteristics of both materials before and after ligand exchange with CoTAPc and before/after oxidation by exposure to air. The left panels in Figure 3 represent the characteristics of the ternary copper chalcogenide NCs, whereas the right

panel characterizes the binary NCs. The color code is the same for both materials: green = OLm capping, reduced; yellow = OLm capping, oxidized; blue = CoTAPc capping, reduced; and red = CoTAPc capping, oxidized. Oxidation leads to copper vacancies and a nonstoichiometric composition in copper selenide NCs and drastically increases the density of free holes, which manifests in degenerate p-type doping as well as the occurrence of an LSPR in the near-infrared (NIR).[10,16,22] Therefore, we monitor the degree of vacancy doping for both samples with vis/NIR absorption spectroscopy in Figure 3c+d. We note a broad band centered at 1250 nm for oxidized $Cu_{2-x}Se_yS_{1-y}$ (for both OLm and CoTAPc ligands), 1300 nm for oxidized OLm-capped $Cu_{2-x}Se$ and 1600 nm for oxidized $Cu_{2-x}Se$ capped with CoTAPc, which we interpret as LSP resonances. In the reduced state, both materials show a negligible LSPR signal below 2000 nm, indicative of a low carrier density and a near stoichiometric copper content. In both ligand-exchanged samples, the singlet transition of CoTAPc invokes a strong absorption band between 600 and 800 nm. (See Supporting Information for the absorption spectrum of pure CoTAPc, Figure S4.) Before ligand exchange, charge transport is poor in both materials (green curve) with conductivities on the order of 10^{-8} S cm^{-1} for $Cu_2Se_yS_{1-y}$ and 10^{-4} S cm^{-1} for Cu_2Se. After surface-functionalization with CoTAPc, both materials behave similar and the conductivities increase dramatically to 1 and 5 S cm^{-1}, respectively (blue curve). In contrast, when studying the effect of oxidation in air for several hours ($Cu_{2-x}Se$) or days ($Cu_{2-x}Se_yS_{1-y}$), we observe a different behavior for $Cu_{2-x}Se_yS_{1-y}$ vs $Cu_{2-x}Se$. While the increase of copper vacancies has a negligible effect on the transport properties of OLm-capped $Cu_{2-x}Se_yS_{1-y}$, it increases the conductivity of the OLm-capped $Cu_{2-x}Se$ to 6 S cm^{-1}. Oxidizing the CoTAPc-capped NC films has no significant effect on the conductivity of either of the two samples (Figure S5).

The structural characterization in Figure 2 demonstrates that the highly conductive OLm-capped $Cu_{2-x}Se$ NCs are well-separated from each other (4.6 ± 1.9 nm), such that necking and the formation of percolative pathways are an unlikely explanation for such efficient charge carrier transport. Similar widths of the OLm ligand sphere are also observed for $Cu_{2-x}Se_yS_{1-y}$ (2.8 ± 0.8 nm, this work) and $Cu_{1.1}S$ NCs (4.1 ± 1.7 nm), which exhibit negligible conductivities (10^{-8} and 10^{-9} S cm^{-1}, respectively).[5] We note that previous reports on drop-casted, oxidized OLm-capped $Cu_{2-x}Se$ NCs revealed similar or even larger conductivities, corroborating our finding here that $Cu_{2-x}Se$ NCs show uniquely different transport properties compared to $Cu_{2-x}Se_yS_{1-y}$ or $Cu_{1.1}S$ NCs.[41–43] It is furthermore surprising that the significant contraction of the $Cu_{2-x}Se$ NC ensemble by 1.7 nm upon ligand exchange has no effect on the conductivity (Figure 3b yellow vs red curve). This speaks against electronic (hopping) conduction as the dominant transport mechanism in OLm-capped $Cu_{2-x}Se$ NC thin films, which is strongly affected by a change of the hopping distance.[53] We hypothesize that ionic conduction of mobile copper ions may play a key role here. Very large ionic mobilities with diffusion constants $>10^{-5}$ cm^2 s^{-1} and superionicity have been reported for $Cu_{2-x}Se$, which can result in electric conductivities >1 S cm^{-1}.[10,54] Although it is not immediately obvious how such ionic conductivity would be affected by the OLm ligand sphere, superionicity is an important feature of $Cu_{2-x}Se$ NCs and likely to be responsible for the unusually large electric conductivities. This would
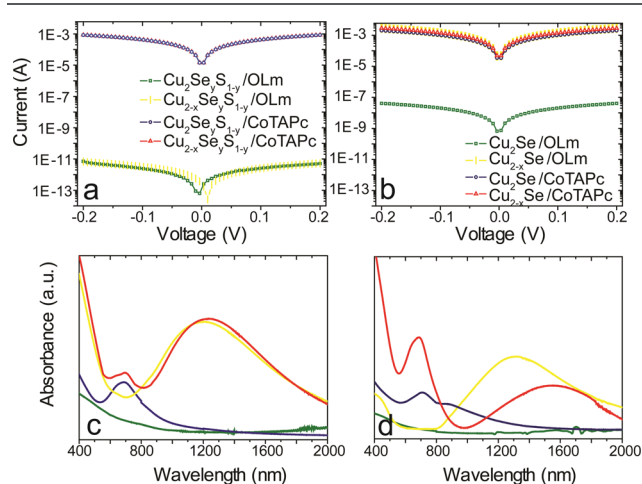
Figure 3. (a) Current−voltage (I−V) curves of $Cu_2Se_yS_{1-y}$ as well as $Cu_{2-x}Se_yS_{1-y}$ and (b) of Cu_2Se and $Cu_{2-x}Se$. (c) Corresponding optical absorption spectra of the ternary and (d) binary copper chalcogenides. The color code is the same in all four panels: green = OLm capping, reduced; yellow = OLm capping, oxidized; blue = CoTAPc capping, reduced; red = CoTAPc capping, oxidized.

explain why only a reduction in copper vacancies can significantly reduce the conductivity in OLm-capped Cu_2Se NCs. After surface-functionalization with CoTAPc, electronic conduction appears greatly improved, such that the conductivity is now only weakly affected by the density of copper vacancies (Figure 3b blue vs red curve).

An alternative explanation which we briefly consider here involves the formation of conductive, percolative pathways consisting of copper oxide nanostructures. Oxidation in air of Cu_2Se NCs results in the release of $Cu(I)$ ions, which react with oxygen to form copper oxide NCs.[16] The conductivity of some copper oxide phases (which are mostly semiconducting) is rather high, and it is possible that successive release of $Cu(I)$ ions from the Cu_2Se NCs leads to a continuous network of this conductor. Once formed, charge transport across this network is expected to be unaffected by the addition of $[Cu(CH_3CN)_4]PF_6$, which is a powerful reducing agent for $Cu_{2-x}Se$ NCs (via filling of $Cu(I)$ vacancies), but not for copper oxide. However, we find that films of $Cu_{2-x}Se$/OLm NCs show a drastically reduced electric conductivity upon treatment with $[Cu(CH_3CN)_4]PF_6$, which speaks against this alternative explanation (see Figure S6).

The transport characteristics of the ternary $Cu_2Se_yS_{1-y}$ NC ensemble appears to be dominated by electronic conduction with a strong dependence on the hopping distance (Figure 3a yellow vs red curve and green vs blue curve) and weak dependence on the density of copper vacancies (Figure 3a green vs yellow curve and blue vs red curve). In view of a recent report on electric transport in similar $Cu_{1.1}S$ NC ensembles, the $Cu_2Se_yS_{1-y}$ NCs investigated here resemble much more of the binary sulfides than the selenides.[5]

To further understand the electronic properties of CoTAPc-capped $Cu_2Se_yS_{1-y}$ NCs, we perform temperature-dependent resistivity measurements under high vacuum (Figure 4a).
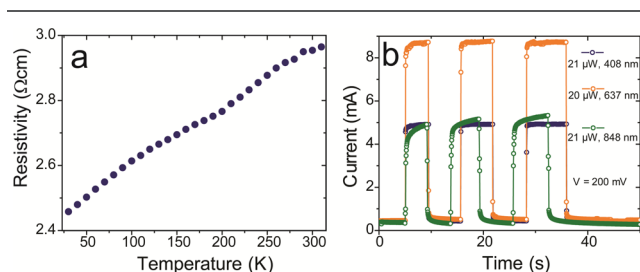
Figure 4. (a) Temperature-dependent resistivity of $Cu_2Se_yS_{1-y}$ functionalized with CoTAPc. (b) Time-dependent current at 200 mV of a $Cu_2Se_yS_{1-y}$/CoTAPc film during three excitation periods to 21 μW of 408 nm light (blue), 20 μW of 637 nm light (orange), and 21 μW of 848 nm (green).

Throughout the entire temperature regime of 20−300 K, we observe monotonically increasing resistance with temperature, reminiscent of metallic behavior. Such a characteristic is rarely observed in copper chalcogenide NC ensembles and only in cases where electronic coupling is large enough to overcome the temperature-activated hopping regime.[34,55]

In light of the tunable optical absorption properties, copper chalcogenide NCs are often considered for applications where light-to-electric current conversion is important, such as photovoltaics or photocatalysis. However, the photocurrent behavior of these materials showed only moderate photo-sensitivities so far.[56−59] In Figure 4b, we display the ON/OFF photocurrent characteristics of $Cu_2Se_yS_{1-y}$/CoTAPc NCs

during three excitation periods with 408, 637, and 848 nm laser diodes at roughly the same direct optical power of ∼20 μW. At a bias of 200 mV, we find a photocurrent of ∼4, ∼8, and 4 mA, respectively, corresponding to a responsivity of 200 A W^{-1} at 408 and 848 nm as well as 400 A W^{-1} at 637 nm. The reversibility of the transport characteristics after each excitation period indicates that the increased current is indeed a photocurrent and not, as recently observed for copper sulfide NCs, an irreversible photodoping effect.[38] We explain such unprecedented optical responsivity with the presence of CoTAPc, which shows strong absorbance at all three excitation wavelengths (see Supporting Information). We suggest that CoTAPc sensitizes $Cu_2Se_yS_{1-y}$ NCs for the absorption of photons at these wavelengths to form singlet excitons in the organic π-system, which are split at the organic−inorganic interface and quickly swept to the source−drain electrodes under a small bias. For comparison, we have also measured the 408 nm photocurrent response for OLm-capped $Cu_2Se_yS_{1-y}$ NCs, that is, without any CoTAPc sensitizers (see Supporting Information Figure S7). Here, the responsivity is only on the order of 3 μA W^{-1}. We conclude that the dramatic increase in responsivity by almost 8 orders of magnitude observed after functionalizing $Cu_2Se_yS_{1-y}$ NCs with CoTAPc is due to the combined effect of better electronic coupling and the additional absorption of the organic π-system. Thus, CoTAPc acts as an electronic cross-linker and optical sensitizer for the NCs.

4. CONCLUSIONS

We have measured the structural, optical, and electric properties of ternary $Cu_2Se_yS_{1-y}$ NC solids capped with oleylamine and the organic π-system cobalt β-tetraaminoph-thalocyanine (CoTAPc), respectively, and compared it to the binary compound Cu_2Se. While the structural and optical response to ligand exchange and oxidation in air is rather similar for both materials, we have observed substantial differences in the charge carrier transport properties. Charge transport in $Cu_2Se_yS_{1-y}$ NC solids is dominated by electronic conduction, very sensitive to structural changes and largely unaffected by oxidation in air. Exchanging the surface ligand oleylamine with the organic π-system not only drastically increases electronic coupling in the $Cu_2Se_yS_{1-y}$ NC ensembles but also invokes an increase in the optical responsivity by 8 orders of magnitude. Thus, ligand exchange with CoTAPc enables high conductivity and large responsivity in $Cu_2Se_yS_{1-y}$ NC films, which are much more robust against oxidation than their binary Cu_2Se analogues.

■ ASSOCIATED CONTENT

ⓢ Supporting Information

The Supporting Information is available free of charge on the ACS Publications website at DOI: 10.1021/acs.chemmater.8b05108.

(S1) XRD pattern of as-synthesized $Cu_2S_ySe_{1-y}$ NCs, (S2) atomic force microscopy images and height profiles of NC films, (S3) Fourier-transform infrared spectra of Cu_2Se and $Cu_2Se_yS_{1-y}$ NC films before and after ligand exchange with CoTAPc, (S4) UV/vis absorption spectrum of pure CoTAPc, (S5) I/V curves of CoTAPc-functionalized $Cu_{2-x}Se_yS_{1-y}$ NCs after varying exposure times to air, (S6) current−voltage character-istics of a Cu_2Se/OLm film after different oxidation/

reduction treatments, and (S7) *I/V* curves of OLm-functionalized $Cu_{2-x}Se_yS_{1-y}$ NCs under photoexcitation by a 408 nm laser diode of varying optical power (PDF)

AUTHOR INFORMATION

Corresponding Author
*E-mail: marcus.scheele@uni-tuebingen.de.

ORCID
Santanu Maiti: 0000-0003-1491-6688
Ali Hossain Khan: 0000-0001-7155-0200
Dirk Dorfs: 0000-0001-6175-4891
Iwan Moreels: 0000-0003-3998-7618
Frank Schreiber: 0000-0003-3659-6718
Marcus Scheele: 0000-0002-2704-3591

Author Contributions
The manuscript was written through contributions of all authors. All authors have given approval to the final version of the manuscript.

Notes
The authors declare no competing financial interest.

REFERENCES

(1) Coughlan, C.; Ibanez, M.; Dobrozhan, O.; Singh, A.; Cabot, A.; Ryan, K. M. Compound Copper Chalcogenide Nanocrystals. *Chem. Rev.* **2017**, *117*, 5865−6109.

(2) Lesnyak, V.; George, C.; Genovese, A.; Prato, M.; Casu, A.; Ayyappan, S.; Scarpellini, A.; Manna, L. Alloyed Copper Chalcogenide Nanoplatelets via Partial Cation Exchange Reactions. *ACS Nano* **2014**, *8*, 8407−8418.

(3) Lynch, J.; Kotiuga, M.; Doan-Nguyen, V. V. T.; Queen, W. L.; Forster, J. D.; Schlitz, R. A.; Murray, C. B.; Neaton, J. B.; Chabinyc, M. L.; Urban, J. J. Ligand Coupling Symmetry Correlates with Thermopower Enhancement in Small-Molecule/Nanocrystal Hybrid Materials. *ACS Nano* **2014**, *8*, 10528−10536.

(4) Liu, L.; Zhou, B.; Deng, L.; Fu, W.; Zhang, J.; Wu, M.; Zhang, W.; Zou, B.; Zhong, H. Thermal Annealing Effects of Plasmonic $Cu_{1.8}S$ Nanocrystal Films and Their Photovoltaic Properties. *J. Phys. Chem. C* **2014**, *118*, 26964−26972.

(5) Maiti, S.; Maiti, S.; Joseph, Y.; Wolf, A.; Brütting, W.; Dorfs, D.; Schreiber, F.; Scheele, M. Electronically Coupled, Two-Dimensional Assembly of $Cu_{1.1}S$ Nanodiscs for Selective Vapor Sensing Applications. *J. Phys. Chem. C* **2018**, *122*, 23720−23727.

(6) Maiti, S.; Sanyal, M. K.; Varghese, N.; Satpati, B.; Dasgupta, D.; Daillant, J.; Carriere, D.; Konovolov, O.; Rao, C. N. R. Formation of Single-Crystalline CuS at the Organic-Aqueous Interface. *J. Phys.: Condens. Matter* **2013**, *25*, No. 395401.

(7) Wang, F.; Li, Q.; Lin, L.; Peng, H.; Liu, Z.; Xu, D. Monodisperse Copper Chalcogenide Nanocrystals: Controllable Synthesis and the Pinning of Plasmonic Resonance Absorption. *J. Am. Chem. Soc.* **2015**, *137*, 12006−12012.

(8) Dilena, E.; Dorfs, D.; George, C.; Miszta, K.; Povia, M.; Genovese, A.; Casu, A.; Prato, M.; Manna, L. Colloidal $Cu_{2-x}(S_ySe_{1-y})$ Alloy Nanocrystals with Controllable Crystal Phase: Synthesis, Plasmonic Properties, Cation Exchange and Electrochemical Lithiation. *J. Mater. Chem.* **2012**, *22*, 13023−13031.

(9) Liu, S.; Zhang, Z.; Bao, J.; Lan, Y.; Tu, W.; Han, M.; Dai, Z. Controllable Synthesis of Tetragonal and Cubic Phase Cu_2Se Nanowires Assembled by Small Nanocubes and Their Electrocatalytic Performance for Oxygen Reduction Reaction. *J. Phys. Chem. C* **2013**, *117*, 15164−15173.

(10) Liu, H.; Shi, X.; Xu, F.; Zhang, L.; Zhang, W.; Chen, L.; Li, Q.; Uher, C.; Day, T.; Snyder, G. J. Copper Ion Liquid-Like Thermoelectrics. *Nat. Mater.* **2012**, *11*, 422−425.

(11) Liu, X.; Wang, X.; Zhou, B.; Law, W.-C.; Cartwright, A. N.; Swihart, M. T. Size-Controlled Synthesis of $Cu_{2-x}E$ (E = S, Se) Nanocrystals with Strong Tunable Near-Infrared Localized Surface Plasmon Resonance and High Conductivity in Thin Films. *Adv. Funct. Mater.* **2013**, *23*, 1256−1264.

(12) Miller, T. A.; Wittenberg, J. S.; Wen, H.; Connor, S.; Cui, Y.; Lindenberg, A. M. The Mechanism of Ultrafast Structural Switching in Superionic Copper (I) Sulphide Nanocrystals. *Nat. Commun.* **2013**, *4*, No. 1369.

(13) Korala, L.; McGoffin, J. T.; Prieto, A. L. Enhanced Conductivity in $CZTS/Cu_{2-x}Se$ Nanocrystal Thin Films: Growth of a Conductive Shell. *ACS Appl. Mater. Interfaces* **2016**, *8*, 4911−4917.

(14) Kriegel, I.; Jiang, C.; Rodriguez-Fernandez, J.; Schaller, R. D.; Talapin, D. V.; da Como, E.; Feldmann, J. Tuning the Excitonic and Plasmonic Properties of Copper Chalcogenide Nanocrystals. *J. Am. Chem. Soc.* **2012**, *134*, 1583−1590.

(15) Wolf, A.; Kodanek, T.; Dorfs, D. Tuning the LSPR in Copper Chalcogenide Nanoparticles by Cation Intercalation, Cation Exchange and Metal Growth. *Nanoscale* **2015**, *7*, 19519−19527.

(16) Dorfs, D.; Hartling, T.; Miszta, K.; Bigall, N. C.; Kim, M. R.; Genovese, A.; Falqui, A.; Povia, M.; Manna, L. Reversible Tunability of the Near-Infrared Valence Band Plasmon Resonance in $Cu_{2-x}Se$ Nanocrystals. *J. Am. Chem. Soc.* **2011**, *133*, 11175−11180.

(17) Marbella, L. E.; Gan, X. Y.; Kaseman, D. C.; Millstone, J. E. Correlating Carrier Density and Emergent Plasmonic Features in $Cu_{2-x}Se$ Nanoparticles. *Nano Lett.* **2017**, *17*, 2414−2419.

(18) Wang, J. J.; Xue, D. J.; Guo, Y. G.; Hu, J. S.; Wan, L. J. Bandgap Engineering of Monodispersed $Cu_{2-x}S_ySe_{1-y}$ Nanocrystals through Chalcogen Ratio and Crystal Structure. *J. Am. Chem. Soc.* **2011**, *133*, 18558−18561.

(19) Balitskii, O. A.; Sytnyk, M.; Stangl, J.; Primetzhofer, D.; Groiss, H.; Heiss, W. Tuning the Localized Surface Plasmon Resonance in $Cu_{2-x}Se$ Nanocrystals by Postsynthetic Ligand Exchange. *ACS Appl. Mater. Interfaces* **2014**, *6*, 17770−17775.

(20) Jain, P. K.; Manthiram, K.; Engel, J. H.; White, S. L.; Faucheaux, J. A.; Alivisatos, A. P. Doped Nanocrystals as Plasmonic Probes of Redox Chemistry. *Angew. Chem., Int. Ed.* **2013**, *52*, 13671−13675.

(21) White, S. L.; Banerjee, P.; Jain, P. K. Liquid-Like Cationic Sub-Lattice in Copper Selenide Clusters. *Nat. Commun.* **2017**, *8*, No. 14514.

(22) Luther, J. M.; Jain, P. K.; Ewers, T.; Alivisatos, A. P. Localized Surface Plasmon Resonances Arising from Free Carriers in Doped Quantum Dots. *Nat. Mater.* **2011**, *10*, 361−366.

(23) Lesnyak, V.; Brescia, R.; Messina, G. C.; Manna, L. Cu Vacancies Boost Cation Exchange Reactions in Copper Selenide Nanocrystals. *J. Am. Chem. Soc.* **2015**, *137*, 9315−9323.

(24) Xie, Y.; Riedinger, A.; Prato, M.; Casu, A.; Genovese, A.; Guardia, P.; Sottini, S.; Sangregorio, C.; Miszta, K.; Ghosh, S.; Pellegrino, T.; Manna, L. Copper Sulfide Nanocrystals with Tunable Composition by Reduction of Covellite Nanocrystals with Cu+ Ions. *J. Am. Chem. Soc.* **2013**, *135*, 17630−17637.

(25) Saldanha, P. L.; Brescia, R.; Prato, M.; Li, H.; Povia, M.; Manna, L.; Lesnyak, V. Generalized One-Pot Synthesis of Copper Sulfide, Selenide-Sulfide, and Telluride-Sulfide Nanoparticles. *Chem. Mater.* **2014**, *26*, 1442−1449.

(26) Xu, J.; Tang, Y.-B.; Chen, X.; Luan, C.-Y.; Zhang, W.-F.; Zapien, J. A.; Zhang, W.-J.; Kwong, H.-L.; Meng, X.-M.; Lee, S.-T.;

Lee, C.-S. Synthesis of Homogeneously Alloyed $Cu_{2-x}(S_ySe_{1-y})$ Nanowire Bundles with Tunable Compositions and Bandgaps. *Adv. Funct. Mater.* **2010**, *20*, 4190−4195.

(27) Cheng, J.; Jia, H.; Lei, Y.; Liu, S.; Gao, Y.; Hou, H.; Zheng, Z. A Facile Room Temperature Route to Ternary $Cu_{7.2}S_2Se_2$ Compounds and Their Photovoltaic Properties Based on Elemental Copper. *Mater. Chem. Phys.* **2017**, *193*, 267−273.

(28) Özel, F.; Sarilmaz, A.; Istanbullu, B.; Aljabour, A.; Kus, M.; Sonmezoglu, S. Penternary Chalcogenides Nanocrystals as Catalytic Materials for Efficient Counter Electrodes in Dye-synthesized solar cells. *Sci. Rep.* **2016**, *6*, No. 29207.

(29) Xu, J.; Yang, X.; Yang, Q.; Zhang, W.; Lee, C. S. Phase Conversion from Hexagonal CuS_ySe_{1-y} to Cubic $Cu_{2-x}S_ySe_{1-y}$: Composition Variation, Morphology Evolution, Optical Tuning, and Solar Cell Applications. *ACS Appl. Mater. Interfaces* **2014**, *6*, 16352−16359.

(30) Xu, J.; Yang, X.; Yang, Q. D.; Huang, X.; Tang, Y.; Zhang, W.; Lee, C. S. Controllable Synthesis of Bandgap-Tunable $CuS_x Se_{1-x}$ Nanoplate Alloys. *Chem. - Asian J.* **2015**, *10*, 1490−1495.

(31) Li, W. L.; Zou, H. Y.; Lan, J.; Wang, Q.; Li, Y. F.; Huang, C. Z. H_2S Bubbles-Assisted Synthesis of Hollow $Cu_{2-x}Se_yS_{1-y}$/Reduced Graphene Oxide Nanocomposites with Tunable Compositions and Localized Surface Plasmon Resonance. *RSC Adv.* **2015**, *5*, 91206−91212.

(32) Zhu, D.; Tang, A.; Kong, Q.; Zeng, B.; Yang, C.; Teng, F. Roles of Sulfur Sources in the Formation of Alloyed $Cu_{2-x}S_ySe_{1-y}$ Nanocrystals: Controllable Synthesis and Tuning of Plasmonic Resonance Absorption. *J. Phys. Chem. C* **2017**, *121*, 15922−15930.

(33) Elimelech, O.; Liu, J.; Plonka, A. M.; Frenkel, A. I.; Banin, U. Size Dependence of Doping by a Vacancy Formation Reaction in Copper Sulfide Nanocrystals. *Angew. Chem., Int. Ed.* **2017**, *56*, 10335−10340.

(34) Otelaja, O. O.; Ha, D. H.; Ly, T.; Zhang, H.; Robinson, R. D. Highly Conductive $Cu_{2-x}S$ Nanoparticle Films through Room-Temperature Processing and an Order of Magnitude Enhancement of Conductivity via Electrophoretic Deposition. *ACS Appl. Mater. Interfaces* **2014**, *6*, 18911−18920.

(35) Lin, Z. Y.; He, Q. Y.; Yin, A. X.; Xu, Y. X.; Wang, C.; Ding, M. N.; Cheng, H. C.; Papandrea, B.; Huang, Y.; Duan, X. F. Cosolvent Approach for Solution-Processable Electronic Thin Films. *ACS Nano* **2015**, *9*, 4398−4405.

(36) Bekenstein, Y.; Elimelech, O.; Vinokurov, K.; Millo, O.; Banin, U. Charge Transport in Cu_2S Nanocrystals Arrays: Effects of Crystallite Size and Ligand Length. *Z. Phys. Chem.* **2015**, *229*, 179−190.

(37) Lee, J.; Yang, J.; Park, C.; Kim, J. H.; Kang, M. S. Electronic Properties of $Cu_{2-x}Se$ Nanocrystal Thin Films Treated with Short Ligand (S^{2-}, SCN^-, and Cl^-) Solutions. *J. Phys. Chem. C* **2016**, *120*, 14899−14905.

(38) Bekenstein, Y.; Vinokurov, K.; Keren-Zur, S.; Hadar, I.; Schilt, Y.; Raviv, U.; Millo, O.; Banin, U. Thermal Doping by Vacancy Formation in Copper Sulfide Nanocrystal Arrays. *Nano Lett.* **2014**, *14*, 1349−1353.

(39) Brewer, A. S.; Arnold, M. S. Field-effect Measurements of Mobility and Carrier Concentration of Cu_2S Colloidal Quantum Dot Thin Films after Ligand Exchange. *Thin Solid Films* **2014**, *567*, 91−95.

(40) Liu, L.; Liu, C.; Fu, W.; Deng, L.; Zhong, H. Phase Transformations of Copper Sulfide Nanocrystals: Towards Highly Efficient Quantum-Dot-Sensitized Solar Cells. *ChemPhysChem* **2016**, *17*, 771−776.

(41) Riha, S. C.; Johnson, D. C.; Prieto, A. L. Cu_2Se Nanoparticles with Tunable Electronic Properties due to a Controlled Solid-State Phase Transition Driven by Copper Oxidation and Cationic Conduction. *J. Am. Chem. Soc.* **2011**, *133*, 1383−1390.

(42) Shen, H.; Wang, H.; Yuan, H.; Ma, L.; Li, L. S. Size-, Shape-, and Assembly-Controlled Synthesis of $Cu_{2-x}Se$ Nanocrystals via a Non-Injection Phosphine-Free Colloidal Method. *CrystEngComm* **2012**, *14*, 555−560.

(43) Deka, S.; Genovese, A.; Zhang, Y.; Miszta, K.; Bertoni, G.; Krahne, R.; Giannini, C.; Manna, L. Phosphine-Free Synthesis of p-Type Copper(I) Selenide Nanocrystals in Hot Coordinating Solvents. *J. Am. Chem. Soc.* **2010**, *132*, 8912−8914.

(44) Vikulov, S.; Di Stasio, F.; Ceseracciu, L.; Saldanha, P. L.; Scarpellini, A.; Dang, Z. Y.; Krahne, R.; Manna, L.; Lesnyak, V. Fully Solution-Processed Conductive Films Based on Colloidal Copper Selenide Nanosheets for Flexible Electronics. *Adv. Funct. Mater.* **2016**, *26*, 3670−3677.

(45) Aigner, W.; Nenova, G. K.; Sliem, M. A.; Fischer, R. A.; Stutzmann, M.; Pereira, R. N. Electronic Changes Induced by Surface Modification of $Cu_{2-x}S$ Nanocrystals. *J. Phys. Chem. C* **2015**, *119*, 16276−16285.

(46) Renaud, G.; Lazzari, R.; Leroy, F. Probing Surface and Interface Morphology with Grazing Incidence Small Angle X-Ray Scattering. *Surf. Sci. Rep.* **2009**, *64*, 255−380.

(47) Jiang, Z. GIXSGUI: a MATLAB Toolbox for Grazing-Incidence X-ray Scattering Data Visualization and Reduction, and Indexing of Buried Three-Dimensional Periodic Nanostructured Films. *J. Appl. Crystallogr.* **2015**, *48*, 917−926.

(48) Maiti, S.; Andre, A.; Banerjee, R.; Hagenlocher, J.; Konovalov, O.; Schreiber, F.; Scheele, M. Monitoring Self-Assembly and Ligand Exchange of PbS Nanocrystal Superlattices at the Liquid/Air Interface in Real Time. *J. Phys. Chem. Lett.* **2018**, *9*, 739−744.

(49) Maiti, S.; Sanyal, M. K.; Jana, M. K.; Runge, B.; Murphy, B. M.; Biswas, K.; Rao, C. N. R. Evidence of Contact Epitaxy in the Self-assembly of HgSe Nanocrystals Formed at a Liquid-Liquid Interface. *J. Phys.: Condens. Matter* **2017**, *29*, No. 095101.

(50) Filippo, E.; Manno, D.; Serra, A. Synthesis and Growth Mechanism of Dendritic $Cu_{2-x}Se$ Microstructures. *J. Alloys Compd.* **2012**, *538*, 8−10.

(51) Ishii, M.; Shibata, K.; Nozaki, H. Anion Distributions and Phase-Transitions in $CuS_{1-x}Se_x (x = 0−1)$ Studied by Raman-Spectroscopy. *J. Solid State Chem.* **1993**, *105*, 504−511.

(52) Kötz, R.; Yeager, E. Raman-Spectroscopy of Cobalt Phthalocyanine Adsorbed on a Silver Electrode. *J. Electroanal. Chem. Interfacial Electrochem.* **1980**, *113*, 113−125.

(53) Scheele, M. To Be or not to Be: Band-Like Transport in Quantum Dot Solids. *Z. Phys. Chem.* **2015**, *229*, 167−178.

(54) Hull, S. Superionics: Crystal Structures and Conduction Processes. *Rep. Prog. Phys.* **2004**, *67*, 1233−1314.

(55) Gao, F.; Leng, S. L.; Zhu, Z.; Li, X. J.; Hu, X.; Song, H. Z. Preparation and Thermoelectric Properties of Cu_2Se Hot-Pressed from Hydrothermal Synthesis Nanopowders. *J. Electron. Mater.* **2018**, *47*, 2454−2460.

(56) Liu, Y.; Dong, Q.; Wei, H.; Ning, Y.; Sun, H.; Tian, W.; Zhang, H.; Yang, B. Synthesis of $Cu_{2-x}Se$ Nanocrystals by Tuning the Reactivity of Se. *J. Phys. Chem. C* **2011**, *115*, 9909−9916.

(57) Choi, J.; Kang, N.; Yang, H. Y.; Kim, H. J.; Son, S. U. Colloidal Synthesis of Cubic-Phase Copper Selenide Nanodiscs and Their Optoelectronic Properties. *Chem. Mater.* **2010**, *22*, 3586−3588.

(58) Geetha, G.; Priya, M.; Sagadevan, S. Investigation of the Optical and Electrical Properties of Tin Sulfide Thin Films. *Chalcogenide Lett.* **2015**, *12*, 609−617.

(59) Kou, H.; Jiang, Y.; Li, J.; Yu, S.; Wang, C. Enhanced Photoelectric Performance of $Cu_{2-x}Se$ Nanostructure by Doping with In^{3+}. *J. Mater. Chem.* **2012**, *22*, 1950−1956.